

Nano-characterization Technique for Steel Research by Using Aberration Corrected Scanning Transmission Electron Microscopy

Genichi SHIGESATO*
Masaaki SUGIYAMA

Shunsuke TANIGUCHI
Yoichi IKEMATSU

Abstract

Nano-characterization of steel by using aberration corrected scanning transmission electron microscopy (STEM) is outlined. The analysis of boron segregation on the prior austenite (γ phase) grain boundary in a boron added steel plate and TiC precipitates in a high strength hot rolled steel sheet were presented. Through these application examples it was found that the aberration corrected STEM was quite useful for nano-characterization in advanced steel.

1. Introduction

In the research and development of the strength, ductility, and other qualities of steel materials, it is important to make a nanometer-order microscopic investigation of such metallurgical phenomena as precipitation, segregation, and phase transformation, which are major factors in controlling the quality of steel materials. In the recent research and development of high-strength, high-function steel materials in particular, structural analysis of steel at the atomic level has been increasingly called for. For example, let us consider transformation strengthening and precipitation strengthening, which are the most widely used metallurgical techniques to increase the strength of steel materials. Transformation strengthening is a technique to control the strength of a steel material by controlling the phase transformation of the steel. It has been known that in controlling phase transformation, the segregation of trace elements added to the steel that occurs in regions having a thickness nearly equal to that of a layer of several atoms (a width less than 1 nm) at the grain boundary or phase interface plays a decisive role.

In precipitation strengthening, the precipitates of a carbide or nitride, etc. are finely dispersed in the steel matrix to increase the strength of the steel material. In this case, the precipitate size and spatial distribution play an important role in controlling the strength of the steel material. In precipitation strengthening for steel materi-

als in particular, the precipitate size that provides the maximum strengthening is normally in the range of several to less than ten nanometers. Therefore, in order to secure an adequate amount of precipitation strengthening by means of precipitation control, information about the distribution, shape, structure, and composition of nano-sized precipitates is indispensable. From this standpoint, it may be said that the research and development of high-strength steel materials requires a nano-characterization technique for the study of various metallurgical phenomena, and that improving existing nano-characterization techniques is an urgent necessity.

Transmission electron microscope (TEM) has come to be widely used as a tool for analyzing the microstructures of steel materials. It is one of the principal analytical devices employed in the research and development of steel materials. Scanning transmission electron microscope (STEM) is a kind of TEM that features a scanning function. Developed more recently, STEM is superior to TEM in its capacity for microstructural observation and elemental analysis of local regions of a specimen. With STEM, which uses electrons transmitted and scattered from the specimen to form an image of the specimen while scanning the electron beam focused onto a narrow spot across the specimen, it is possible not only to directly observe the atomic structure of the grain boundary, phase interface, and precipitate, but also to observe an image of the specimen where the contrast is directly related to the atomic number. In addition, by detecting

* Chief Researcher, Ph.D., Materials Characterization Research Lab., Advanced Technology Research Laboratories 20-1, Shintomi, Futtso, Chiba

signals from the characteristic x-rays and suchlike emitted from the specimen, it is possible to analyze the composition of the specimen. When synchronized with the electron beam scanning function, elemental mapping can easily be performed.

In image observation or elemental analysis using TEM or STEM, a beam of electrons is irradiated onto and scanned across the specimen, and the electrons that pass through the specimen are used to form an image of the specimen. In so doing, the path of the electron beam is controlled using an electromagnetic lens. However, the electromagnetic lens is subject to aberrations, such as spherical aberration and chromatic aberration, which impose certain restrictions on image resolution and spatial resolution in elemental analysis with a conventional TEM/STEM. With an ordinary TEM/STEM (acceleration voltage: 200 kV to 300 kV), the image resolution is no more than approximately 0.2 nm with a spatial resolution in elemental analysis of no more than approximately 1 nm.

Aberration-corrected STEM has a built-in mechanism for correcting unwanted spherical aberration of the irradiation lens system to condense the beam of electrons. Thanks to this mechanism, it is possible to eliminate spherical aberration almost completely.¹⁻³⁾ As a result, both image resolution and spatial resolution in elemental analysis improve to 0.1 nm or less. Therefore, it is expected that the aberration-corrected STEM will allow for sub-nanometer-level analysis of nano-sized precipitates and grain boundary segregations in steel materials.⁴⁾

This paper describes the aberration-corrected STEM system that is expected to play a vital role in the nano-characterization of steel materials. In addition, it presents examples of applications of the aberration-corrected STEM in analytical tasks on an atomic level, such as the analysis of nano-sized precipitates in a steel material and the measurement of concentration profiles of trace elements added to a steel material and segregated at its grain boundary.

2. Principles and Configuration of Aberration-corrected STEM

Fig. 1 shows the configuration of the aberration-corrected STEM that was used in the present study. In a TEM/STEM, the aberration corrector is provided in the irradiation system or in the imaging system. In the case of a STEM, the aberration correction of the lens of the irradiation system is especially important since image resolution and spatial resolution in elemental analysis depend on the degree to which the beam of electrons irradiated onto the specimen can be converged. In the case of a TEM, by contrast, in order to allow for high-resolution image observation, it is important to image as accurately as possible the electron beam intensity distribution formed at the bottom of the specimen as a result of the interaction between the electron beam and the specimen. Therefore, in an aberration-corrected TEM, the aberration of the lens of the imaging system is corrected. In addition, there is an electron microscope called a “double corrector,” which is provided with an aberration correction mechanism in both the irradiation system and the imaging system.

For the aberration-corrected STEM used in the present study, a spherical aberration corrector of the irradiation system was adopted since major importance was attached to the elemental analysis function. The aberration corrector is installed under the lens of the irradiation system. The concept of correction of the spherical aberration of a lens can roughly be explained by using a convex lens and a concave lens (Fig. 2). The electromagnetic lens that performs the function of a convex lens concentrates a beam of electrons on the specimen. On the specimen surface, broadening (off-focus), expressed

as δ_s , of the electron beam occurs because of spherical aberration of the lens.

$$\delta_s = C_s \alpha^3 \tag{1}$$

Here, C_s denotes the spherical aberration coefficient of the object lens, and α denotes the aperture angle of the object lens. With conventional STEMs, the beam broadening expressed by Equation 1 cannot be avoided because of the spherical aberration of the lens of the irradiation system and hence, spatial resolution in elemental analysis is no more than approximately 1 nm.

With the aberration-corrected STEM, which is provided with an aberration corrector corresponding to the concave lens in Fig. 2, it is possible to eliminate the above spherical aberration almost completely by adjusting the function of the concave lens so that it cancels out the spherical aberration of the convex lens. This makes it possible to improve spatial resolution in elemental analysis to 0.1 nm or less, allowing for composition analysis with atomic-level resolution.

The acceleration voltage of the STEM used in the present study can be varied between 80 kV and 300 kV. In the case of steel materials, a higher acceleration voltage is often advantageous since they transmit electron beams less easily than semiconductors, such as silicon or organic materials composed mainly of carbon. The high acceleration voltage of 300 kV makes it possible to observe even speci-

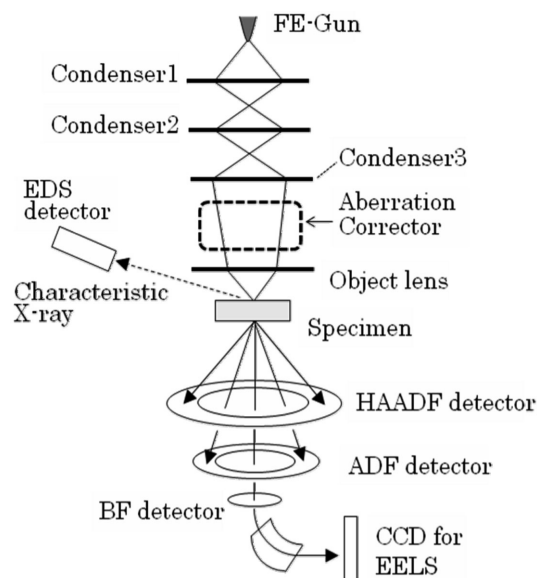


Fig. 1 Configuration diagram of aberration corrected STEM

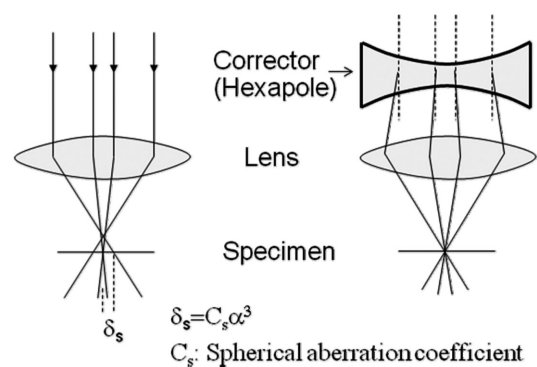


Fig. 2 Conceptual diagram of aberration correction

mens that are relatively thick (up to $0.2 \mu\text{m}$). It also permits dislocation structures to be observed and in-situ observations to be performed. On the other hand, a beam of electrons accelerated with such high voltage can damage the specimen. In particular, when the beam of electrons is narrowed down to the atom-size level for image observation or elemental analysis, damage to the specimen caused by the electron beam may become a serious problem. In such cases, it is better to use a lower acceleration voltage. When the acceleration voltage is no more than 100 kV, it seldom causes damage to a steel specimen. In view of the aforementioned, the broad acceleration voltage range of 80 kV to 300 kV is extremely effective for analyzing steel materials.

When it comes to implementing image observation or elemental analysis with such an ultrahigh resolution as 0.1 nm or less, not only is the equipment performance described above important, but so too are the equipment installation conditions. Floor vibration, room temperature fluctuation, voltage change, magnetic field variation, noise, etc. are among the factors that impair the stability of the equipment. Our aberration-corrected STEM is operated in an environment completely free from such external disturbances. As a result, it enables an image resolution of 0.1 nm or less on a reliable basis.

3. Application of the Aberration-corrected STEM in the Nano-characterization of Steel Materials

3.1 Observation of high-resolution STEM images

In order to evaluate the image resolution of our aberration-corrected STEM, we observed high-angle annular dark-field (HAADF) images of silicon and steel (Fe-0.1%C-1.5%Mn-0.5%Si). The observation results are shown in Fig. 3.

HAADF is an observation technique whereby electrons dispersed from the specimen at a high angle are detected by an annular detector for image formation. In an observation of STEM images, the beam of electrons is narrowed down to atom size and the orientation of the specimen is finely adjusted so that the direction of incidence of the electron beam is parallel to the atomic rows. When the electron beam is irradiated onto an atomic row, it is strongly dispersed. When the electron beam is irradiated between atomic rows, however, it is hardly dispersed at high angles. As a result, it is possible to observe images of the atomic array. With this technique, unlike the case of high-resolution TEM images, the positions of atoms, not the lattice pattern produced by the interference of an electron beam, are observed directly. Therefore, it is easy to observe the array of atoms even in a region where the periodic structure is disturbed, as in at the grain boundary. In addition, since the high-angle dispersion intensity is proportional to the square of the atomic number, it is possible to

observe images that strongly reflect the atomic number (the heavier the element, the brighter the image).

It should be noted, however, that HAADF images are obtained by scanning a narrow beam of electrons across a specimen. Therefore, in order to observe an image of the atomic array, it is necessary that (i) the electron beam is able to be condensed to atomic size or smaller and that (ii) the electron beam and the specimen are stable at the atomic level during image acquisition (acquiring a single image normally takes several tens of seconds). In other words, if an image of the atomic array can be observed as an HAADF image, it is proof that the electron beam diameter is no larger than the atomic size, that the electron beam step width is invariable, and that the specimen is stationary at the atomic level.

Fig. 3 (a) and (b) show HAADF images of a single silicon crystal obtained when a beam of electrons was irradiated from [110]. In the image (Fig. 3 (a)) obtained with a conventional STEM (acceleration voltage: 200 kV) owned by Nippon Steel Corporation, the array of silicon atoms cannot be clearly observed owing in part to the influence of the installation site conditions (floor vibration, etc.). By contrast, in the image obtained with the aberration-corrected STEM (Fig. 3 (b)), the array of silicon atoms can be clearly observed across the field of vision. Fig. 3 (c) is an enlarged view of the central part of Fig. 3 (b). It shows in high contrast pairs of silicon atoms in the shape of dumbbells. Since the distance between the two silicon atoms in each pair is 0.136 nm, it can be seen that the rows of silicon atoms are observed with very high spatial resolution.

The resolution of the HAADF images evaluated by means of Fourier transform was approximately 0.09 nm. It took about 40 seconds to obtain each of the high-resolution HAADF images. Since the images obtained are almost free of fluctuation, it can be seen that the electron beam was scanned very stably. This means that composition analysis on an atomic level described in the next section can be carried out accurately since neither off-positioning of the electron beam nor drifting of the specimen occurs during measurement. As shown in Fig. 3 (d), it is also possible to observe a high-resolution HAADF image of α -Fe (the electron beam irradiated from [111]). Thus, it was confirmed that the aberration-corrected STEM could effectively be applied to the nano-characterization of steel materials as well.

3.2 Composition analysis of nano-sized TiC precipitates in steel

As described in Chapter 1, nano-sized precipitates contribute to precipitation strengthening in improving the strength of steel materials. Therefore, characterizing nano-sized precipitates is important. In this section, the results of analysis of nano-sized TiC precipitates in a steel material are discussed.

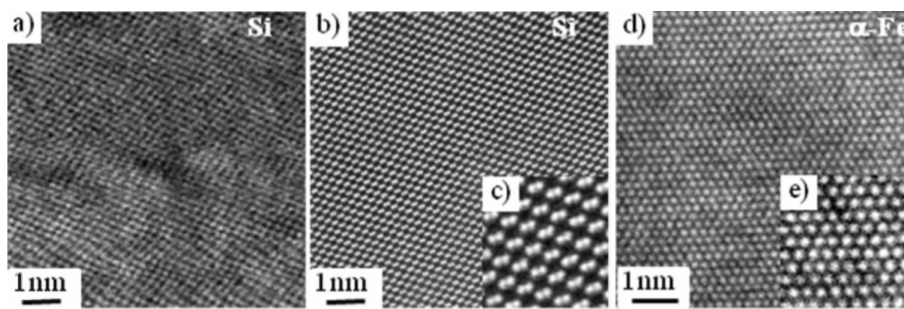


Fig. 3 HAADF images of Si and α -Fe

(a)Si observed from [110] with conventional STEM, (b),(c)Si observed from [110] with aberration corrected STEM, (d),(e) α -Fe from [111] with aberration corrected STEM

We attempted to observe precipitates in precipitation-hardened, dual-phase steel by using the aberration-corrected STEM. As the name indicates, the steel consists of two phases—martensite and ferrite. If the difference in hardness between the hard martensite phase and the soft ferrite phase is excessive, a fracture can originate in the martensite-ferrite interface, causing steel workability to deteriorate. In this respect, by precipitation-hardening the ferrite phase, it is possible to reduce the difference in hardness between the two phases and thereby improve the workability of the steel. The chemical composition of the steel material that was observed and analyzed is shown in **Table 1**. A steel ingot of the composition shown was subjected to hot rolling, cold rolling, and annealing in a continuous annealing furnace. The hot rolling, cold rolling, and annealing conditions are shown in **Fig. 4**. The steel material thus manufactured was reduced in thickness to 50 to 70 μm by mechanical and chemical polishing and punched into disks 3 mm in diameter. The disks were then made into specimens for TEM/STEM observation by electrolytic polishing. The strength of the steel material measured by a tensile test exceeded 1,200 MPa. Thus, the steel material exhibited very high strength.

Fig. 5 shows an STEM bright-field image of the steel material observed at relatively low magnification. The dark portions are mar-

Table 1 Chemical compositions of the precipitation hardened dual phase steel

(mass%, * ppm)				
C	Si	Mn	Ni	B*
0.15	1.72	2.09	3.0	10

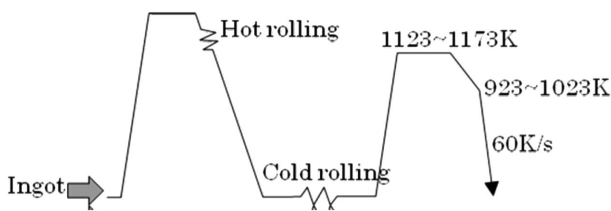


Fig. 4 Manufacturing process of the steel used for the observation of precipitates

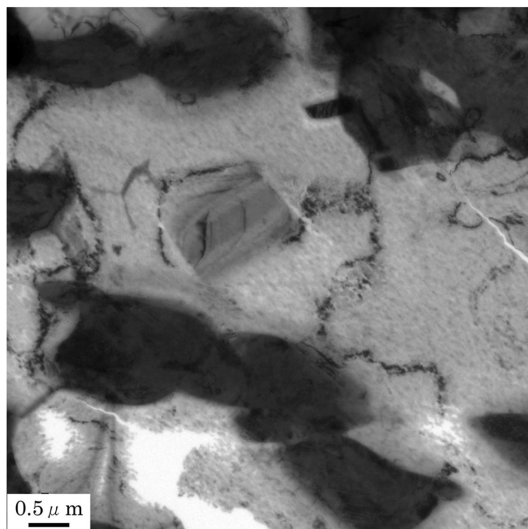


Fig. 5 Microstructure of the precipitation hardened dual phase steel (STEM bright field image at low magnification)

tensite grains, and the bright portions are ferrite grains. It can easily be seen from the image that the steel material has a dual-phase (martensite-ferrite) structure. Observation of the ferrite grains at high magnification reveals many fine precipitates as shown in **Fig. 6**. **Fig. 7** shows an electron energy-loss spectroscopy (EELS) spectrum obtained by irradiating a beam of electrons onto the central part of a precipitate. The presence of a Ti peak indicates the presence of Ti precipitates. An EELS spectrum at each of the points scanned by the electron beam was obtained, and the Ti peak intensity obtained from each of the EELS spectra was used to prepare a Ti mapping image, which is shown in **Fig. 8**. From the above observation results, it can be seen that Ti precipitates approximately 5 nm in size were dispersed in the ferrite grains.

As has been described above, by using an aberration-corrected STEM, it is possible to observe the microstructure of steel continuously from relatively low magnification to very high magnification corresponding to atomic-level resolution. This means that the aber-

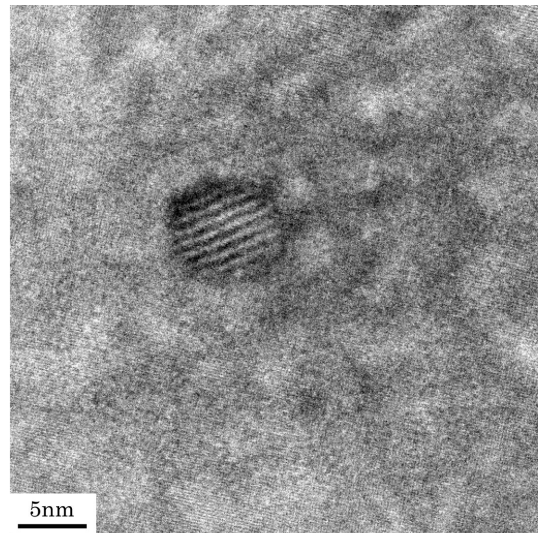


Fig. 6 STEM bright field image of the precipitate in ferrite phase

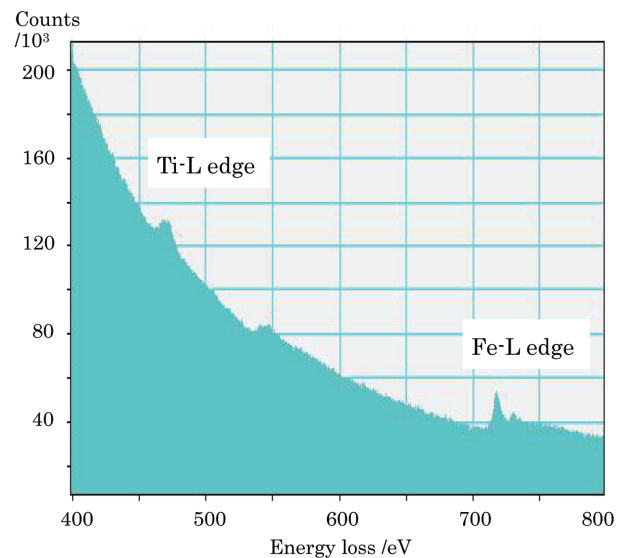


Fig. 7 EELS spectrum obtained from the precipitate in ferrite phase

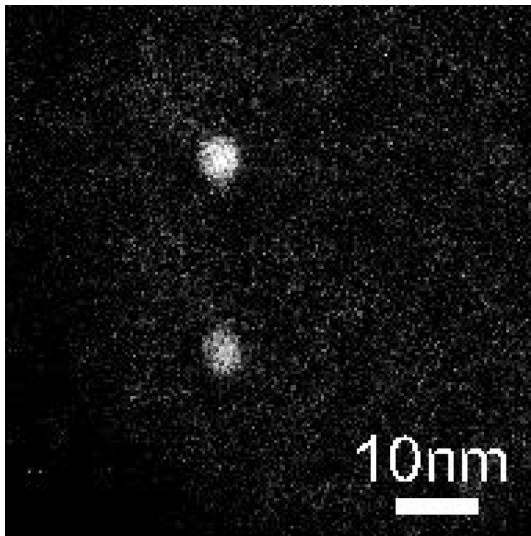


Fig. 8 EELS-Ti mapping image of the precipitate in ferrite phase

ation-corrected STEM makes it possible to analyze the condition of dispersion and the composition of nano-sized precipitates in steel.

3.3 Measurement of the concentration profiles of boron segregation at grain boundaries

It is already known that when a small amount of B is added to steel, the hardenability and strength of the steel improve.⁵⁾ The improvement in hardenability by the addition of B manifests itself when the concentration of B is only several parts per million (ppm). Since the addition of B permits reduction in the amounts of Ni, Mo, Cr, and other costly alloying elements added to secure the desired hardenability of steel, it can be expected that B will make it possible to manufacture high-strength steel at lower cost. Therefore, B is positioned to be one of the most important elements in the development of high-strength steel materials.

The reason that the hardenability of steel improves when a small amount of B is added to the steel is considered to be as follows. While the steel is in an austenite (γ) phase at high temperature, B segregates at the grain boundary (γ grain boundary), thereby restraining the ferrite (α) transformation that takes place at the grain boundary while the steel is cooled. When transformation to the α phase is restrained, martensite and bainite structures are formed. As a result, the steel is strengthened. Several analytical techniques have been used in an attempt to grasp the segregation of B at the γ grain boundary. For example, secondary ion mass spectroscopy (SIMS) has been used to observe the segregation of B in the neighborhood of the prior γ grain boundary.⁶⁾ However, because of the insufficient spatial resolution of SIMS, the condition of B's existence (i.e., whether B is in precipitate form or exists as a solid solution) in the neighborhood of the grain boundary is unknown. In order to restrain α transformation, it is necessary that B should exist in the form of a solid solution at the grain boundary. Therefore, the information required to clarify the transformation behavior cannot be obtained using SIMS.

In measurement using an atom probe,⁷⁾ B could be detected with high spatial resolution. However, quantitative information about its transformation behavior could not be obtained because of the difficulty involved in measurement focused on the γ grain boundary. An attempt has also been made to carry out local analysis of B using a conventional STEM. However, because of the limited spatial reso-

lution in the analysis, it was difficult to detect B segregation in the γ grain boundary or to quantitatively measure the B distribution in the vicinity of the grain boundary. Under these conditions, we considered using the aberration-corrected STEM to measure B, which was considered likely to segregate in the vicinity of the γ grain boundary.

The chemical composition of the steel subjected to experiment is shown in Table 2. A base steel (Fe-0.05%C-1.5%Mn) with 11-ppm B added and 0.5% Mo was made into an ingot in a vacuum melting furnace. The ingot was heat-treated as shown in Fig. 9. After the ingot was held at 1,223 K for 60 seconds, it was cooled down to 923 K at a rate of 30 K/s. We assumed that by so doing, non-equilibrium B segregation,^{8,9)} whereby B is distributed over a relatively wide range around the γ grain boundary, would occur. In addition, the steel was quenched from 923 K for martensite transformation from the γ phase so that the location of the γ grain boundary at high temperatures remained the same as at room temperature. The grain boundary thus obtained is a martensite grain boundary, which is called a prior γ grain boundary since it was formerly a γ grain boundary. From the above steel material, a region (approximately $10 \times 10 \times 3 \mu\text{m}$) containing a prior grain boundary was extracted using focused ion beam (FIB) equipment. It was then fixed on a grid made of Mo and reduced in thickness to $0.1 \mu\text{m}$ or less. The specimens thus obtained were analyzed under the STEM.

Fig. 10 shows STEM dark-field images of one of the thin specimens. The prior γ grain boundary is seen near the center of the image. Line analysis was conducted across the prior grain boundary with an electron probe scanned on the line indicated by a white line. The probe size of the electron beam used in the analysis was 0.1 to 0.2 nm. Fig. 11 shows an EELS spectrum obtained from a region right above the grain boundary. A peak (B-K edge) indicating the presence of B can be clearly observed at an energy loss of around 188 eV. Fig. 12 shows the B concentration obtained from the EELS

Table 2 Chemical compositions of B added steel

(mass%, * ppm)								
C	Mn	S*	Ni	Mo	Ti	Al	N*	B*
0.05	1.50	5	3.0	0.5	0.006	0.03	15	11

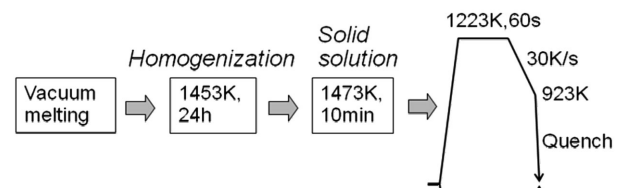


Fig. 9 Manufacturing process of the steel used for the measurement of B segregation

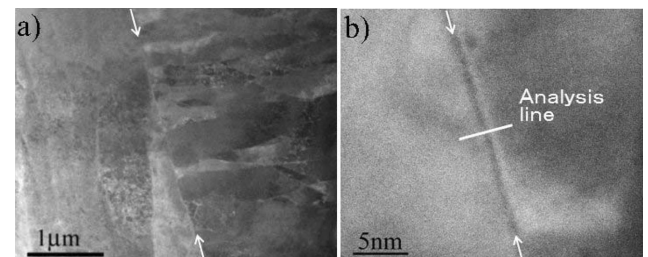


Fig. 10 STEM dark field images of the prior γ grain boundary in B added steel

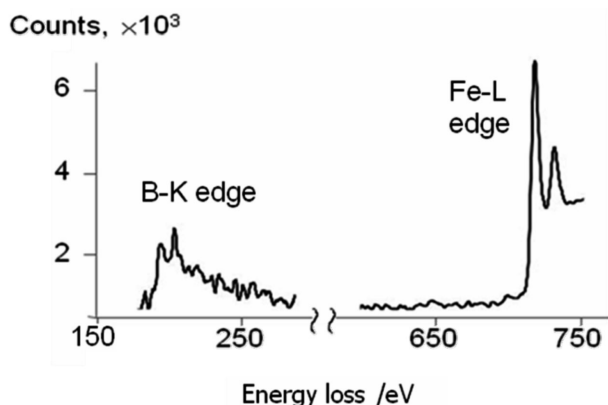


Fig. 11 EELS spectrum obtained from the prior γ grain boundary

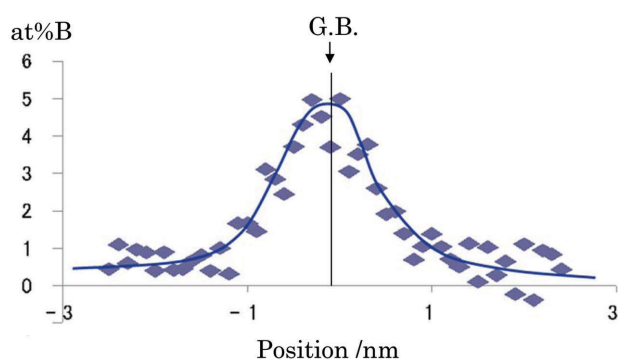


Fig. 12 Example of B profiles measured around the grain boundary

spectrum at each of the measuring points and plotted against the distance from the grain boundary. It is evident from the graph that B segregates on and near the prior γ grain boundary. The concentration of B at the grain boundary is as high as approximately 6 at%.

The above results clearly indicate that B segregates in the prior γ grain boundary. However, in order to clarify the mechanism whereby the addition of B restrains α transformation, it is necessary to quantitatively evaluate the concentration of B at the grain boundary and the B concentration distribution in the vicinity of the grain boundary. To this end, the quantitative performance of the measurement of B concentrations by STEM-EELS must be studied. The factors considered likely to influence the B concentrations measured by this method include: the angle of inclination of the grain

boundary to the electron beam; broadening of the beam of electrons in the specimen; background correction of the EELS spectrum; and the cross-sectional area of each element used in converting the signal intensity of the EELS spectrum into the concentration, etc. At present, our study group is attempting to quantitatively evaluate the influences of the above factors and accurately grasp the concentration distribution of B in and around the grain boundary.¹⁰⁾

4. Conclusion

In this paper, we outlined the principles of an aberration-corrected STEM and the configuration of the aberration-corrected STEM system introduced to Nippon Steel Corporation. In addition, we presented examples of applications of the STEM in the analysis of precipitation and segregation, etc., which have become important issues in the study of various metallurgical phenomena with steel materials. Furthermore, we showed that it is possible to analyze and measure the microstructures of steel materials with a resolution in the order of sub-nanometers. In the future, we intend to press ahead with the application of the aberration-corrected STEM in the study of steel materials and to tackle the development of a specimen preparation technique to bring aberration-corrected STEM performance into full play, improvement in the quantitative performance of elemental analysis techniques such as EELS and EDS (energy-dispersive X-ray spectroscopy), and sophistication of the HAADF image quantitative interpretation technique, etc. so that aberration-corrected STEM technology will play a central role as nano-characterization technology demanded for the development of next-generation steel materials. We also consider it possible to accelerate the pace of research and development of steel materials by promoting the application of the aberration-corrected STEM to complement the three-dimensional atom probe equipment that plays such an important role in atomic-level analyses at Nippon Steel Corporation.

References

- 1) Haider, M. et al.: Nature. 392, 768 (1998)
- 2) Dellby, N. et al.: J. Electron Microsc. 50, 177 (2001)
- 3) Batson, P. E., Dellby, N., Krivanek, O. L.: Nature. 418, 617 (2002)
- 4) Abe, E., Lupini, A., Pennycook, S. J.: Electron Microscopy. 38, 142 (2003)
- 5) Shyne, J. C., Morgan, E. R., Frey, D. N.: Trans. ASM. 48, 265 (1956)
- 6) Karlsson, L. et al.: Acta Metall. 36, 25 (1988)
- 7) Karlsson, L. et al.: Acta Metall. 36, 35 (1988)
- 8) Tingdong, Xu., Shenhua, S., Zhexi, Y.: Acta Metall. 37, 319 (1989)
- 9) Karlsson, L. et al.: Acta Metall. 36, 25 (1988)
- 10) Shigesato, G., Fujishiro, T., Taniguchi, S., Hara, T., Ikematsu, Y., Sugiyama, M.: Proceedings of the 17th International Microscopy Congress. 2010, M8-8



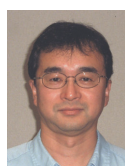
Genichi SHIGESATO
Senior Researcher, Ph.D.,
Materials Characterization Research Lab.,
Advanced Technology Research Laboratories
20-1, Shintomi, Futtsu, Chiba



Shunsuke TANIGUCHI
Researcher,
Materials Characterization Research Lab.,
Advanced Technology Research Laboratories



Masaaki SUGIYAMA
Chief Researcher, D.Eng.,
Materials Characterization Research Lab.,
Advanced Technology Research Laboratories



Yoichi IKEMATSU
Chief Researcher, D.Eng.,
Materials Characterization Research Lab.,
Advanced Technology Research Laboratories